# Transition of the Future Precipitation Types in the Tianshan Mountains Region, China

**Rui Ren** ( renrui232@163.com )
Lanzhou Jiaotong University https://orcid.org/0000-0002-6391-4737
**Xuemei Li**
Faculty of Geomatics, Lanzhou Jiaotong University, Lanzhou 730070, China;
**Lanhai Li**
Xinjiang Institute of Ecology and Geography, Chinese Academy of Sciences, Urumqi 830011, China;
**Yiyu Huang**
Faculty of Geomatics, Lanzhou Jiaotong University, Lanzhou 730070, China;

**Research Article**

**Keywords:** Tianshan Mountains region, precipitation types, CMIP5 models, BP neural network

**Posted Date:** March 16th, 2021

**DOI:** https://doi.org/10.21203/rs.3.rs-283927/v1

# Transition of the future precipitation types in the Tianshan Mountains region, China

Rui Ren[1,3,4], Xuemei Li[1,3,41], Lanhai Li[2], Yiyu Huang[1,3,4]

[1] Faculty of Geomatics, Lanzhou Jiaotong University, Lanzhou 730070, China;
[2] Xinjiang Institute of Ecology and Geography, Chinese Academy of Sciences, Urumqi 830011, China;
[3] National-Local Joint Engineering Research Center of Technologies and Applications for National Geographic State Monitoring, Lanzhou, 730070, China;
[4] Gansu Provincial Engineering Laboratory for National Geographic State Monitoring, Lanzhou, 730070, China

**Abstract.** The general circulation models (GCMs) from the coupled model intercomparison project phase 5 (CMIP5) were used to evaluate the simulation capabilities of rainfall-to-precipitation ratio (RPR) from 1961 to 2018 at 28 meteorological stations in the Tianshan Mountains region (TMR). Moreover, it was estimated the change of RPR in the months experiencing freezing-thawing transitions from 2011 to 2100 under three representative concentration pathways (RCPs), RCP2.6, RCP4.5, and RCP8.5. The results indicated that the simulated air temperature from CMIP5 was highly correlated with the observed values, while the performance for precipitation was poor. Therefore, it is feasible to forecast the future RPR employing the temperature provided by CMIP5 and the observed meteorological factors by the BP neural network (BNN). Under three emission scenarios, the RPR in the months experiencing freezing-thawing transitions during 2011-2100 will increase compared to that during the baseline period (1981-2010). Under the same emission scenario, values of RPR will increase as the time goes on. Besides, in terms of spatial variation, values of RPR in the south slope will be larger than that in the north slope under three emission scenarios. Furthermore, values of RPR exhibit different variation characteristics under different emission scenarios. Under the RCP2.6 emission scenario, as the time goes on, values of RPR at more stations will change slightly. Under the RCP4.5 emission scenario, the increase of RPR will occur in the whole TMR and stabilize in the north slope by the end of this century. However, values of RPR will increase significantly through 21$^{st}$ century in the whole TMR under the RCP8.5 emission scenario.

**Keywords:** Tianshan Mountains region; precipitation types; CMIP5 models; BP neural network.

[1] Corresponding author: Xuemei Li
E-mail: lixuemei@lzjtu.edu.cn

# 1 Introduction

Precipitation falls on the ground in various forms such as rain, snow, and sleet, and each type of them has an important impact on surface runoff and energy balance (Loth et al. 1993). The surface albedo increases sharply when snowfall occurs, which leads to a decrease in solar radiation absorbed from the ground (Cohen and Rind 1991). In the meantime, snowfall is stored on the ground surface as snow cover, subsequently melts and recharges river runoff as temperatures rise in the spring (Clark et al. 2006). Conversely, when rainfall occurs, it quickly infiltrates and collects into rivers or groundwater, which has the opposite effect of snowfall (Dai and Aiguo 2008). Therefore, the differentiation of precipitation types is important for land hydrological process management (Anderson and Mackintosh 2012).

Historical meteorological data revealed that the earth experienced a warming trend both globally and locally (Chen et al. 2016; Ghosh 2018; Huang et al. 2018; IPCC 2013; IPCC et al. 2018; Ogunbode et al. 2019). The fastest warming occurred in the mid-latitudes of the northern hemisphere with the increasing rate of temperature exceeded 0.4℃/10a on average (Ji et al. 2014). The average warming rate of China was significantly higher than that of the northern hemisphere over the same period. Warming mainly occurred in winter and spring. And compared with Northern and Eastern China, the warming rate of Northwest China was even higher (Li et al. 2015), e. g., the Tianshan Mountains region (TMR) of Xinjiang located in Northwest China. The TMR divide Xinjiang into two parts, i. e., Southern Xinjiang and Northern Xinjiang. Due to its unique topographic features of mountains, basins, and valleys, the TMR is particularly sensitive to global climate change (Guo and Li 2015; Li et al. 2019).

In the arid and semi-arid regions of Northwest China, water resources mainly come from the mountain area. Roughly 373 rivers originate from the TMR. Thus it is typically referred to as a "solid reservoir" (Hu 2004; Wang et al. 2014). Although the total area of TMR accounts for less than 17% of the area of Xinjiang, its precipitation accounts for about 40% of the total precipitation in Xinjiang (Xu et al. 2014). Moreover, winter snowfall in the Western TMR accounts for more than 30% of annual precipitation (Li et al. 2019; Lu et al. 2016). Within the last 50 years, there was a significant trend of overall warming and local humidifying in the TMR (Li et al. 2016). If different types of precipitation are transformed, it will inevitably affect the process of regional runoff generation and confluence, as well as the annual distribution of runoff (Feng and Hu 2004).

Global warming has led to change in global precipitation types. The rise of temperature showed a trend of decreasing snowfall and increasing rainfall in the western part of the United States from 1949 to 2004 (Knowles et al. 2006). The frequency of different precipitation types generally increased with increasing temperature in winter, but the number of snowfall days in spring decreased more significantly with increasing temperature than that of rainfall days in northern Eurasia

from 1936 to 1990 (Ye and Hengchun 2008). The ratio of rainfall to precipitation increased significantly during spring to summer on the Canadian Arctic Island from 1979 to 2015 (Wei et al. 2018). The average ratio of snow to precipitation (S/P) showed a downward trend with precipitation and snowfall rise as well as temperatures rise in the cold season in the TMR from 1961 to 2010 (Guo and Li 2015). Therefore, given the important impact of precipitation types on the climate and the abnormality of the precipitation types in the context of global warming, the possible change in precipitation types in the future are a very worthy concern.

The simulation ensemble of the general circulation models (GCMs) from the coupled model intercomparison project phase 5 (CMIP5) has become the main tool in future climate change assessment (Hussain et al. 2017; Jing et al. 2017; Noor et al. 2019). The IPCC Fifth Report (AR5) Global Climate Change Future Prediction Experiment used the greenhouse gas emission scenario proposed by the IPCC expert group, called the representative concentration pathway (RCP). The AR5 of IPCC shares four typical concentration paths, namely RCP8.5, RCP6.0, RCP4.5 and RCP2.6 (IPCC 2013). In predicting the future climate using the CMIP5 model, most studies focus on estimating the total amount of precipitation without distinguishing precipitation types. However, there are also some researches concerning prediction of conversion of precipitation types using CMIP5 model in the TMR. It was found that a significant decrease in snowfall and a significant increase in rainfall under the RCP4.5 and RCP8.5 scenarios, by the end of the 21$^{st}$ century (Jing et al. 2017).

CMIP5 models have a better performance for simulating temperature in Northwest China, but poor for simulating precipitation (Dandan et al. 2018; Lu et al. 2020). The change of RPR was most closely related to temperature (Rui et al. 2020). BP Neural Network (BNN) is a useful tool for predicting various climate variables (ASCE 2000). Considering the relationship between temperature and the Rainfall-to-Precipitation Ratio (RPR), the future temperature under different RCPs provided by CMIP5 models and the meteorological factors from meteorological stations was inputted into the BNN model to acquire the future RPR.

The objectives of this study were to: (1) evaluate the performance of CMIP5 model to simulate the temperature and precipitation in the TMR, (2) calculate the values of RPR in the months experiencing freezing-thawing transitions in the future, and (3) analyze the temporal and spatial change of RPR in the TMR in the future. This study may provide a scientific management basis for agricultural production and hydrology, as well as change in the water cycle in alpine region under climate change.

## 2 Study area and data description

### 2.1 Study area

The TMR extends 1700 km from the border between China and Kyrgyzstan in the west to the Xingxingxia Gobi in the east to Hami city with area of about 5.7 × 105 km$^2$ accounting for more than 34.5% of the total area of Xinjiang (1.65 × 106 km$^2$) (Hu 2004) (Fig.1). It is located in the deep inland of Eurasia and far away from the ocean

with the temperate continental climate. Composed of mountains, mountain basins, valleys, and piedmont plains, the average altitude of the TMR is 4000 m. Affected by the westerly belt and terrain, the precipitation shows an uneven spatial and temporal distribution in the TMR. For instance, the precipitation in the north slope is more than that in the south slope. And the precipitation in the mountains is also more than that in the plains and basins.

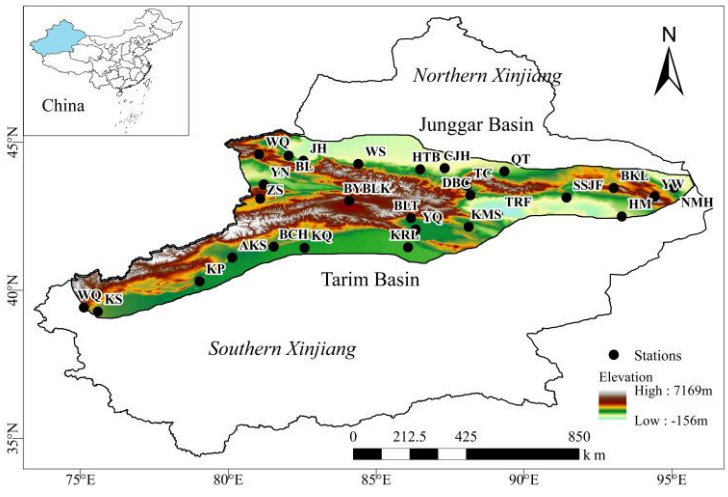


**Fig. 1.** Map of the TMR and the distribution of selected meteorological stations

## 2.2 Data used

### 2.2.1 Observation data

As the change of precipitation types mainly occur in the months experiencing freezing-thawing transitions, this study mainly focused on the change of precipitation types in 4 months, October and November before winter, and March and April after winter. The observed data during 1960-2018 from 28 meteorological stations in TMR (Fig. 1) including daily precipitation, average temperature, relative humidity, average pressure, average wind speed, sunshine hours, and small evaporation data were obtained from the National Meteorological Information Center in China (http://data.cma.cn). In addition, terrain factors data including altitude, slope, aspect, longitude and latitude data were obtained from a 30-meter-resolution digital elevation model (DEM) provided by the Geo-spatial Data Cloud in China (http://www.gscloud.cn).

### 2.2.2 CMIP5 models

Temperature and precipitation grid data from 21 GCM models of CMIP5 (Table 1) were selected, including annual and monthly data (https://esgf-node.llnl.gov/projects/cmip5/). The annual grid data during 1961-2018 were used for adaptability assessment of GCM models. The monthly grid data were used to statistically downscale to the meteorological station for the base period and the future period. 1981-2010 was as the base period, and 2011-2100 as the future period. Most models failed to perform prediction experiments under the RCP6.0 scenario. Therefore, this study selected RCP2.6, RCP4.5, and RCP8.5 as the future climate scenarios. And the resolution was uniformly interpolated to 1°×1°.

**Table 1.** Basic information of the CMIP5 models selected in this study

| Identifier | Model name | Modeling center country and abbreviation | Horizontal resolution (lon × lat) |
|---|---|---|---|
| 1 | BCC-CSM1-1 | BCC, China | 128×64 |
| 2 | BCC-CSM1-1-m | BCC, China | 320×160 |
| 3 | BNU-ESM | GCESS, China | 128×64 |
| 4 | CanESM2 | CCCMA, Canada | 128×64 |
| 5 | CCSM4 | NCAR, USA | 288×192 |
| 6 | CESM1-CAM5 | NSF-DOE-NCAR, USA | 288×192 |
| 7 | CNRM-CM5 | CNRM-CERFACS, France | 256×128 |
| 8 | CSIRO-Mk3-6-0 | CSIRO-QCCCE, Australia | 192×96 |
| 9 | EC-EARTH | EC-EARTH, Ten European countries | 320×160 |
| 10 | FGOALS-g2 | FGOALS, China | 128×60 |
| 11 | GFDL-ESM2G | NOAA GFDL, USA | 144×90 |
| 12 | GFDL-ESM2M | NOAA GFDL, USA | 144×90 |
| 13 | HadGEM2-AO | NIMR/KMA, Korea/UK | 192×145 |
| 14 | HadGEM2-ES | MOHC, UK | 192×145 |
| 15 | IPSL-CM5A-LR | IPSL, France | 96×96 |
| 16 | IPSL-CM5A-MR | IPSL, France | 144×143 |
| 17 | MIROC5 | MIROC, Japan | 256×128 |
| 18 | MIROC-ESM | MIROC, Japan | 128×64 |
| 19 | MIROC-ESM-CHEM | MIROC, Japan | 128×64 |
| 20 | MRI-CGCM3 | MRI, Japan | 320×160 |
| 21 | NorESM1-M | NCC, Norway | 144×96 |

# 3 Methodology

## 3.1 Schemes of distinguish precipitation

The China Meteorological Administration has more than 643 reference meteorological stations throughout the country. And the precipitation data were marked with precipitation types from January 1951 to December 1979, but not marked after 1980 (Han et al. 2010). Therefore, Ding proposed a set of parameterization schemes to distinguish precipitation types (Ding et al. 2014). That is, the model scheme constructed by the observation data from 824 stations marked with precipitation types from 1951 to 1979 were used to distinguish the precipitation types after 1980.

## 3.2 Calculation of precipitation types

Rainfall-to-Precipitation Ratio (RPR) is defined as the percentage of rainy days to total precipitation days:

$$\mathrm{RPR} = \frac{R}{P} \times 100\% \tag{1}$$

In the formula, $R$ and $P$ denote the total rainfall days and the total precipitation days during the study period, respectively. This paper mainly studies the changing characteristics of precipitation types in the TMR through the change of RPR. The values of RPR have a range from 0 to 1. Among them, RPR approaching to 0 indicates the tendency of precipitation from the liquid to the solid, while RPR approaching to 1 means that the trend of precipitation from the solid to the liquid.

## 3.3 Downscaling model

CMIP5 models could better simulate the characteristics of meteorological elements at large-scale with a low spatial resolution. It tends to ignore small-scale differences and is difficult to make detailed predictions of regional climate scenarios. Generally, the error is reduced by downscaling. It can convert large-scale global climate models into small-scale and regional climate models, thereby obtaining more accurate climate data.

The Delta method is a relatively simple but commonly used method to downscale GCMs. Relative change is selected for precipitation, that is, the grid cumulative precipitation in a certain month during a certain year from GCMs is compared with the average cumulative precipitation in a certain month over many years under three emission scenarios. And the change rate of precipitation was obtained for each station. The average accumulated precipitation in a certain month from each meteorological station during the base period is multiplied by change rate of precipitation. Then the cumulative precipitation data for a certain year and month under three emission scenarios were obtained. The temperature choice is absolute change. The difference values between average temperature in a certain month during a certain year and the

average temperature in a month for many years of grid data from GCMs under three emission scenarios were calculated. And this amount of change was added to the monthly average temperature at meteorological station within the grid during the base period measured for many years. Then the average temperature data of a certain year and month under three emission scenarios could be obtained for a certain station (Hay et al. 2010). The method is as follows:

$$P_f = P_o \frac{P_{Gf}}{P_G} \tag{2}$$

$$T_f = T_o + (T_{Gf} - T_G) \tag{3}$$

where $P_o$ is the measured average cumulative precipitation in a certain month for many years. $P_G$ is the simulated cumulative average precipitation in a certain month for many years in the future. $P_{Gf}$ is the simulated cumulative future precipitation in a certain month of a certain year. $P_f$ is the cumulative monthly precipitation under three emission scenarios obtained by the Delta method. $T_o$ is the measured average temperature of a certain month for many years. $T_G$ is the average temperature of a certain month for many years under three emission scenarios. $T_{Gf}$ is used to simulate the average temperature of a certain month during a certain year under three emission scenarios. And $T_f$ is the average monthly temperature under three emission scenarios to be obtained by the Delta method.

The monthly data from 21 GCMs (1°×1°) were interpolated to stations through the bilinear interpolation method. Based on the base period from 1961 to 2000, the monthly data under three emission scenarios from 2011 to 2100 was downscaled through the Delta method.

### 3.4 BNN model

The artificial neural network model is based on the research of neuroscience and reflects some basic characteristics of human brain function and proposes a method of using neural networks. So far, lots of artificial neural networks have been developed. Among them, the most widely used one is the multi-layer perception neural networks. Its research started in the 1950s, but there had been no progress until 1986 Rumelhart proposed the learning representations by back-propagating errors (BP calculation) (Fig. 2), which realized Minsky's multi-layer network idea (Rumelhart et al. 1986).

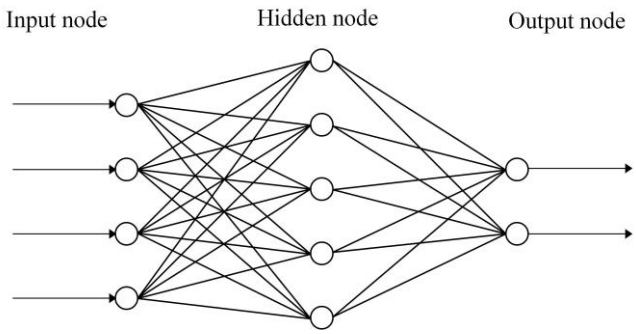


**Fig. 2.** Learning representations by back-propagating errors

The BP algorithm has not only input layer nodes and output layer nodes but also more than one hidden layer node. The input signal needs to be first propagated to the hidden layer node after the action function. Then the output signal of the hidden layer node is propagated to the output node. Finally, the output was provided. As shown in formula (4), the node's action excitation function usually chooses S-type.

$$f(x) = \frac{1}{1 + e^{-x/Q}} \tag{4}$$

Here, $Q$ is the Sigmoid parameter adjusted in the form of an excitation function. The learning process of the algorithm consists of forwarding propagation and back-warding propagation. In the forwarding propagation process, the input information is processed from the input layer through the hidden layer and then passed to the output layer. The state of each layer of the neuron only affects the state of the next layer of the neuron. If the output layer does not obtain the target output, it will be transmitted to the back-warding propagation. And the error signal will return along the original connection channel. By changing the weights of neurons in each layer, the error signal is minimized.

## 3.5 Verification of model accuracy

### 3.5.1 Evaluation of CMIP5 models

To evaluate the performance of the CMIP5 models in simulating the temperature and precipitation in the TMR, the Taylor Diagram was used in this study. In this diagram, three transformation indexes of the correlation coefficient, standard deviation, and root-mean-square error between two fields or two sequences can be placed on the same polar coordinate chart. It uses the triangular transformation relationship to comprehensively reflect the optimization of the simulation results of each model inferior. Specifically, the spatial correlation coefficient between the simulation result sequence and the observation sequence can represent the ability to describe the main center position. The standard deviation of the observation sequence indicates the ability of the model to

simulate the center amplitude. The closer value of the standard deviation is to 1, the better the simulation ability is. The root-mean-square error indicates the similarity between the simulation type and the observed values. And the closer value of the root-mean-square error is to 0, the better the simulation ability is.

### 3.5.2 BNN model accuracy verification

To verify the accuracy of the BNN model simulation, the Nash-Sutcliffe coefficient (NSC) (Nash and Sutcliffe 1970), root-mean-square error (RSR), and percentage bias (PBIAS) were used for quantitative analysis. The theoretical range of NSC is from -∞ to 1. And NSC with a value greater than 0 is used as an indicator to evaluate the consistency between the observed value and the estimated value. When the value of NSC approaches to 1, the predicted value approaches to the observed value (Moriasi et al. 2007). The range of RSR is from 0 to +∞. The lower value of the RSR means the better simulation ability of the model. PBIAS evaluates whether the predicted value is less than or greater than the corresponding observation to assessment the performance of the model. Positive value indicates that the model is underestimated. And negative value indicates that the model is overestimated (Gupta et al. 1999). If the NSC value is greater than 0.5, the RSR value is less than 0.7 and the absolute values of PBIAS is less than 30%, the simulation results are satisfactory (Table **2**) (Moriasi et al. 2007). The calculation formulas for each indicator are as follows:

$$NSC=1-\frac{\sum_{i=1}^{N}(y_i-\hat{y}_i)^2}{\sum_{i=1}^{N}(y_i-\bar{y})^2} \quad (5)$$

$$RSR=\frac{\sqrt{\frac{\sum_{i=1}^{N}(y_i-\hat{y}_i)^2}{N}}}{\sqrt{\frac{\sum_{i=1}^{N}(y_i-\bar{y})^2}{N}}} \quad (6)$$

$$PBIAS=\frac{\sum_{i=1}^{N}(y_i-\hat{y}_i)\times 100}{\sum_{i=1}^{N}y_i} \quad (7)$$

Where $y_i$, $\hat{y}_i$, $\bar{y}$, and $N$ is the observed value, the predicted value, the average of the observed data and the number of observations, respectively.

**Table 2.** Basic information of the CMIP5 models selected in this study

| Performance rating | Grades | NSC | RSR | PBIAS (%) |
|---|---|---|---|---|
| Very good | A | 0.75<NSC≤1 | 0≤RSR≤0.5 | PBIAS<±15 |

| | | | | |
|---|---|---|---|---|
| Good | B | 0.65<NSC≤0.75 | 0.5<RSR≤0.6 | ±15≤PBIAS<±20 |
| Satisfactory | C | 0.50<NSC≤0.65 | 0.6<RSR≤0.7 | ±20≤PBIAS<±30 |
| Unsatisfactory | D | NSC≤0.50 | RSR>0.7 | PBIAS≥±30 |

# 4. Results

## 4.1 Evaluation of CMIP5 models

To quantitatively compare the simulating ability of the CMIP5 models for the temperature and precipitation in the TMR, Fig. 3 provided an illustration of the Taylor Diagram for the annual cumulative precipitation and the annual average temperature from the 21 CMIP5 models relative to the observation stations during 1961-2018. It can be seen from Fig. 3 that the scope of spatial correlation coefficients between the simulation and observation were from -0.26 to 0.74 for the annual cumulative precipitation. And the scope of standard deviation between simulation and observation were during 0.84-1.90 mm. Whereas, for the annual average temperature, the scope of spatial correlation coefficients between simulation and observation were 0.84-0.98. And the scope of the standard deviation between the simulation and observation were 0.93-1.13°C. Most of the root-mean-square error between the simulation and observation were greater than 1 for annual cumulative precipitation, but the root-mean-square error between simulation and observation were less than 1 for the annual average temperature. In general, the CMIP5 models had a high correlation between the simulated and the observed temperature. But the performance of precipitation was poor.

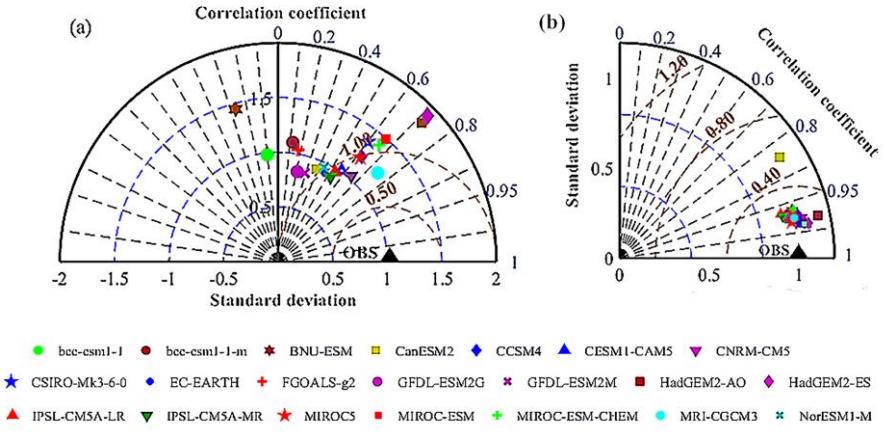

**Fig. 3.** Taylor Diagram of the 21 CMIP5 models simulated fields and the observed fields: (a) annual precipitation and (b) annual mean temperature during period (1961- 2018) in TMR

### 4.2 The verification of BNN model

Because the CMIP5 model had a better ability to simulate the temperature compare to the precipitation in the TMR. Hence, the future precipitation data provided by CMIP5 were abandoned, while the future temperature data provided by CMIP5 combined with the BNN model could be used to predict the future RPR in the TMR. That is, the meteorological factors related to RPR in one certain month, such as air temperature, average pressure, evaporation, relative humidity, wind speed, sunshine hours, and surface temperature were used as input variables, and RPR for one certain month was used as the output variable. The data during 1961-1999 and the data during 2000-2018 were selected as the calibration and the verification, respectively. NSC, RSR, and PBIAS were used to assess the performance for the calibration and verification.

Table 3 provided the performance for the calibration and verification of the monthly RPR from 28 meteorological stations using the BNN model in the TMR. It can be seen that the performance values were all satisfactory and above. Consequently, this model could be ulteriorly used to simulate the future monthly RPR. Change of RPR was most closely related to temperature (Rui et al. 2020). It was assumed that other meteorological factors in the model were unchanged, and that only temperature change significantly. Based on the relationship between air temperature and RPR, using the future monthly average temperature under different RCPs from 21 CMIP5 models as the inputs, the monthly RPR under different RCPs could be obtained by the BNN model.

**Table 3.** Performance for the calibration and verification of the RPR from 28 meteorological stations using the BNN model in the TMR

| | Station | Abridge | NSC(C/V) | RSR(C/V) | PBIAS(C/V) | Rating |
|---|---|---|---|---|---|---|
| 1 | Aksu | AKS | 0.90/0.82 | 0.46/0.49 | -0.25/1.35 | A/A |
| 2 | Baicheng | BCH | 0.79/0.70 | 0.46/0.56 | 1.32/-1.32 | A/B |
| 3 | Bole | BL | 0.81/0.71 | 0.43/0.56 | -0.16/-1.70 | A/B |
| 4 | Barkol | BKL | 0.66/0.61 | 0.58/0.64 | 0.20/8.60 | B/C |
| 5 | Baluntai | BLT | 0.65/0.60 | 0.62/0.68 | 0.00/-1.51 | C/C |
| 6 | Bayinbuluke | BYBLK | 0.85/0.80 | 0.32/0.46 | 0.01/-0.23 | A/A |
| 7 | Caijiahu | CJH | 0.70/0.69 | 0.59/0.54 | 1.20/-2.30 | B/B |
| 8 | Dabancheng | DBC | 0.86/0.78 | 0.44/0.49 | -2.68/-1.52 | A/A |
| 9 | Hami | HM | 0.76/0.62 | 0.38/0.51 | 3.61/5.36 | A/B |
| 10 | Hutubi | HTB | 0.71/0.66 | 0.60/0.54 | -5.44/9.30 | B/B |
| 11 | Jinghe | JH | 0.70/0.63 | 0.54/0.64 | -2.3/-1.65 | B/C |
| 12 | Kuqa | KQ | 0.80/0.76 | 0.41/0.49 | 0.08/0.36 | A/A |
| 13 | Korla | KRL | 0.80/0.76 | 0.49/0.50 | -0.78/-1.25 | A/A |
| 14 | Kumishen | KMS | 0.72/0.65 | 0.61/0.68 | 0.40/6.23 | C/C |
| 15 | Kalpin | KP | 0.71/0.64 | 0.58/0.61 | 0.00/-0.32 | B/C |
| 16 | Kashi | KS | 0.68/0.58 | 0.56/0.61 | 2.64/6.23 | B/C |
| 17 | Naomaohu | NMH | 0.89/0.85 | 0.39/0.42 | 0.01/0.12 | A/A |

| | | | | | | |
|---|---|---|---|---|---|---|
| 18 | Qitai | QT | 0.69/0.56 | 0.51/0.68 | 3.20/-3.21 | B/C |
| 19 | Shisanjianfang | SSJF | 0.85/0.80 | 0.42/0.46 | 0.00/-0.31 | A/A |
| 20 | Tianchi | TC | 0.68/0.57 | 0.62/0.66 | 0.36/-3.20 | B/C |
| 21 | Turpan | TRF | 0.90/0.85 | 0.41/0.49 | 0.00/-2.82 | A/A |
| 22 | Wenquan | WQ | 0.75/0.54 | 0.57/0.61 | 0.00/-1.72 | B/C |
| 23 | Wusu | WS | 0.78/0.64 | 0.47/0.63 | -0.85/-0.41 | A/C |
| 24 | Wuqia | WUQ | 0.69/0.59 | 0.56/0.62 | 2.87/5.75 | B/C |
| 25 | Yining | YN | 0.66/0.68 | 0.59/0.52 | 2.36/-0.41 | B/B |
| 26 | Yanqi | YQ | 0.70/0.60 | 0.62/0.69 | 0.32/-3.20 | C/C |
| 27 | Yiwu | YW | 0.72/0.66 | 0.52/0.58 | 0.00/-1.71 | B/B |
| 28 | Zhaosu | ZS | 0.71/0.81 | 0.52/0.67 | 0.22/0.57 | B/A |

## 4.3 Prediction of precipitation types in the future

### 4.3.1 Trends of RPR in the future

The BNN model predicted the RPR under different emission scenarios as shown in Fig. 4 Under three emission scenarios, the RPR in the months experiencing freezing-thawing transitions from 2011 to 2100 will be higher than that during the baseline period (1981-2010) in the TMR. And the values of RPR under the RCP2.6, RCP4.5 and RCP8.5 emission scenarios will increase by 4.36%, 8.27%, and 12.36%, respectively. The values of RPR will mostly increase with the rise of emission scenario.

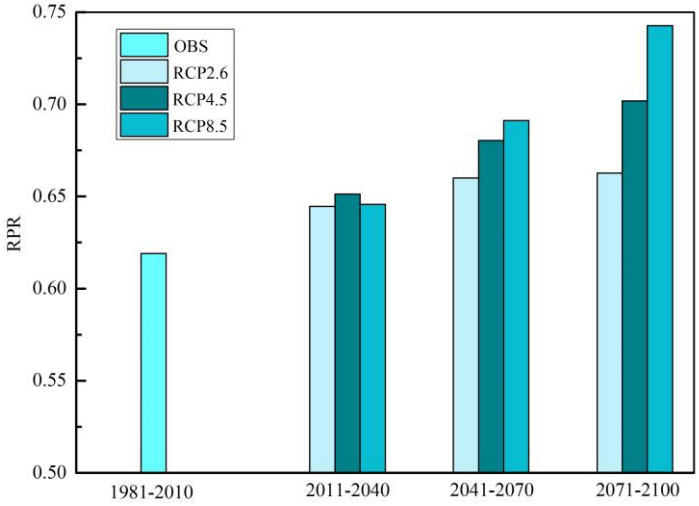

**Fig. 4.** RPR in the months experiencing freezing-thawing transitions under different scenarios (RCP2.6, 4.5, and 8.5) in the TMR

#### 4.3.2 The intra-annual pattern of RPR in the future

Due to the complex terrain of the TMR, the RPR from different stations varies in the same month. Taking Tianchi station at a higher altitude and Bole station at a lower altitude as examples, the box-plot was used to analyze change of RPR in months experiencing freezing-thawing transitions under different emission scenarios during the historical period of 1981-2010 and the future period of 2071-2100 (Fig.5).

Bole station is located in 531.9 meters above sea level. The values of RPR in April and October were 1.00 during the historical period, and the RPR values will be still 1.00 during the future period. The change of RPR mainly occurred in March and November, closer to winter. The lower edge and lower quartile of RPR were 0 in March during the historical period with the range of 0-0.5. During the future period, the range of RPR will have a tight distribution under the RCP2.6 emission scenario. Its lower quartile will vary from 0 to 0.3, and the upper quartile will be slightly lower than the historical period. The low quartile of RPR will increase to 0.34 and 0.42 under the RCP4.5 and RCP8.5 emission scenario, respectively. The overall distribution of RPR tends to move to 1.00. Both of the lower edge and lower quartile of RPR were 0 in November and March during the historical period. But the distribution of RPR in November were mainly concentrated during 0-0.24, more concentrated than that in March. The lower edge and lower quartile of RPR under RCP2.6 and RCP4.5 emission scenario will be only increase weakly in the future. And the upper edge and upper quantile of RPR under RCP2.6 emission scenario remain the same as the historical period. The overall distribution range of RPR will increase to 0.12-0.47 under the RCP8.5 emission scenario.

Tianchi station has a high altitude of 1942.5 meters. Its temperature is low and the RPR values in March and November were 0 during the historical period. During the future period, in addition to a great increase of RPR under the RCP8.5 emission scenario, the increase of RPR will be slight under the RCP2.6 and RCP4.5 emission scenario with values lower than 0.2. The change of RPR will mainly occur in warmer April and October with range of 0.17-0.44. During the future period, the change of RPR under the three emission scenarios will be larger than that during historical period. And the range of the lower quartile will be mostly higher than that of the upper quartile during the historical period. The lower edge and lower quartile of RPR were 0, and the upper quartile was 0.36 in November during the historical period. The distribution of RPR under the three emission scenarios during the future period will be tighter than that during the historical period. The distribution range of RPR under RCP2.6 emission scenario will be similar to that under RCP4.5 emission scenario, ranging from 0.32 to 0.48. The range of RPR will be relatively high under RCP8.5 emission scenario, ranging from 0.42 to 0.56.

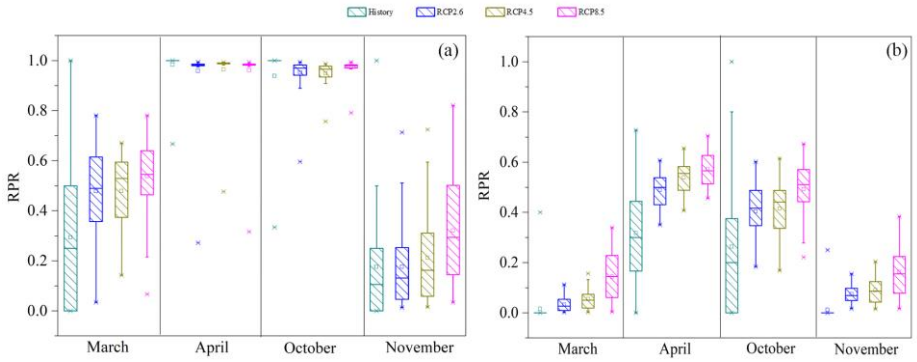


**Fig. 5.** Box plots of RPR under three emission scenarios at (a) Bole and (b) Tianchi station during historical periods (1981-2010) and the future periods (2071-2100)

#### 4.3.3 Spatial distribution of RPR in the future

The continuous spatial distribution was obtained by the Kriging method to interpolate values of RPR in the months experiencing freezing-thawing transitions under different emission scenarios from 28 meteorological stations in the TMR (Fig.6). During 1981-2010, the largest value of RPR occurred at Turpan station with the value of 0.97, while the smallest one happened at Bayinbuluke station with the value of 0.12. Values of RPR in the south slope were larger than that in the north slope. The RPR values ranged from 0.24 to 0.71 in the north slope, while the RPR values ranged from 0.47 to 0.97 in the south slope. The spatial distribution of RPR during 2011-2040, 2041-2070, and 2071-2100 will be similar to that during 1981-2010 with the pattern of "the RPR values in the south slope are larger than that in the north slope".

Under the RCP2.6 emission scenario, the values of RPR in the whole study area will have a slightly increasing trend. By the end of the 21$^{st}$ century, the RPR values will get up to 0.98 and 0.17 at Turpan station and Bayinbuluke station, respectively. The range of RPR will be from 0.44 to 0.77 in the north slope, while the range of RPR values will be from 0.54 to 0.98 in the south slope. Under the RCP4.5 emission scenario, the RPR values will get up to 1.00 and 0.20 at Turpan and Bayinbuluke station by the end of this century, respectively. The range of RPR values will increase to 0.47-0.77 in the north slope and 0.59-1.00 in the south slope. Under the RCP8.5 emission scenario, the RPR values will increase to 0.47-0.83 in the north slope and 0.65-1.00 in the south slope. RPR values will reach to 1.00 at Turpan station during 2041-2070.

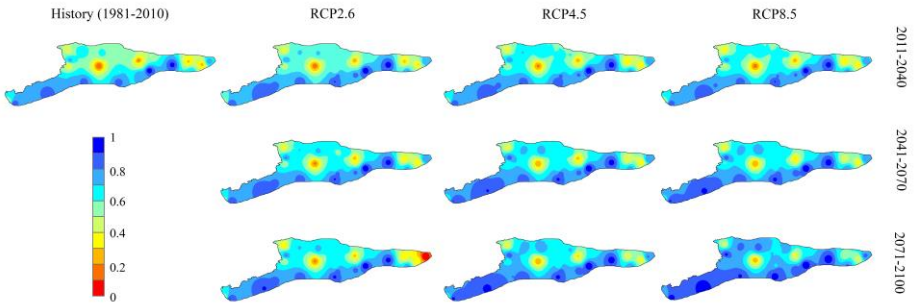


**Fig. 6.** Spatial distribution of RPR in the months experiencing freezing-thawing transitions under RCP2.6, 4.5, and 8.5 emission scenario in the TMR

#### 4.3.4 The changing trend of RPR in the future

From 1981 to 2010, the values of RPR exhibited an increasing trend in the months experiencing freezing-thawing transitions at 28 meteorological stations in the TMR. And the significant increase of RPR at the 0.05 significance level occurred at 6 stations (Fig.7). Among them, the increase rate of RPR in the north slope were larger than that in the south slope. And the increase rate was 0.01/10a in the north slope. There were 5 stations with no changing trend in the entire study area.

Compared with the period of 1981-2010, the values of RPR under the three emission scenarios (RCP2.6, RCP4.5, and RCP8.5) from 2011 to 2040 showed increasing trends in the TMR. And there will be 15, 18, and 19 stations with significant increasing trends at the 0.05 significance level under the three emission scenarios, respectively. However, the increase rate of RPR showed different characteristics under the three emission scenarios during 2041-2070. Under the RCP2.6 emission scenario, except for the decrease of RPR at Qitai station and the increase of RPR at Yiwu station, and values of RPR will remain unchanged at other stations. Under the RCP4.5 emission scenario, except for the decrease of RPR at Qitai station and the unchanged of RPR at Bayinbuke and Wusu station, the increase will take place at the other stations. There will be 17 stations with significant increase at the 0.05 significance level. The changing feature of RPR under the RCP8.5 emission scenario will be similar to that under the RCP4.5 emission scenario. And there will be 15 stations with an increase rate of more than 0.05/10a at the 0.05 significance level. The change of RPR also exhibit different characteristics under the three emission scenarios during 2071-2100. Under the RCP2.6 emission scenario, the decrease of RPR will occur at Wenquan and Qitai station. And the significant decrease will occur at Wenquan station at 0.05 significance level. The slight increase of PRP will take place at four stations with increase rate less than 0.05/10a. The values of RPR will change slightly at the other stations. Under the RCP4.5 emission scenario, the values of RPR will change slightly in the north slope. While significant increase will take place in the south slope at the 0.05 significance level. Under the RCP8.5 emission scenario, the RPR will show a decreasing trend at Qitai station. Except for the unchanged at Yining, Bayinbuke, and Wusu station, the

significant increasing trend will occur at remaining 22 stations at the 0.05 significance level,

The changing feature of RPR during the future period are different from that during the historical period in the TMR. Specifically, under the RCP2.6 emission scenario, as time goes on, more stations will change slightly. And the low-emission scenario makes the trend of RPR tend to stabilize. Under the medium-emission scenario, RPR will increase in the whole region and eventually stabilized in the north slope. Under high-emission scenario a significant increase of RPR will take place in the whole region during all periods.

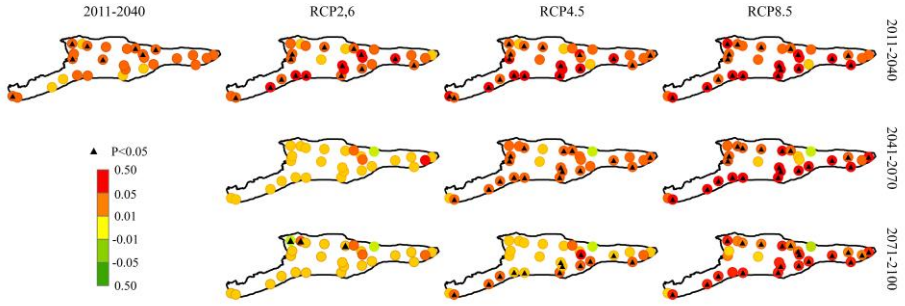


**Fig. 7.** Spatial distribution of changing trend of RPR in the months experiencing freezing-thawing transitions in TMR under the three emission scenarios (RCP2.6, 4.5, and 8.5)

Note: The results have passed the 95% reliability t-test (black triangle)

## 5. Discussion

The TMR is water source in the arid region of Xinjiang, China. The local people considered it as view of "Xinjiang water comes from Tianshan Mountains". In recent years, a great number of studies have been carried out on the spatial and temporal distribution of precipitation, precipitation intensity and frequency in this region (Chen et al. 2016; Li et al. 2016). With global warming, Xinjiang has shown its special "warming and humidifying" characteristics, which have changed types of precipitation. It has affected the regional water resources production and confluence process as well as annual distribution (Li et al. 2016). Therefore, the prediction of precipitation types and their transition in the future under different emission scenarios can provide theoretical support for the early prevention of spring flood disasters and the protection of solid water resources in the arid and semi-arid area of Northwest China.

This study used the future temperature data provided by CMIP5 and multiple meteorological factors data to predict the RPR through the BNN model mainly because CMIP5 could better simulate the temperature data in the TMR. The performance of precipitation in the TMR is still poor even though after downscaling. It's similar to the result that CMIP5 model could better simulate temperature than precipitation in arid inland river basin (Qi et al. 2017). And it is also consistent with the result that the

performance for maximum temperature and the minimum temperature was well but for precipitation was poor in the Kaidu River Basin using data of HadCM3 model (Dandan et al. 2018). Furthermore, Ren identified the key driving factors for the change of RPR in the TMR using meteorological factors (barometric pressure and air temperature, etc.), topographic factors (elevation and aspect, etc.), and geographical factors (longitude and latitude) (Rui et al. 2020). It is obtained that air temperature is the key driving factor affecting transition of precipitation types. Since air temperature plays a leading role in the transformation of precipitation types, other meteorological factors only play a weak role. Therefore, in the prediction of future RPR, it is reasonable to suppose that only the temperature change and other factors remain unchanged as time goes on.

In the forecast of future RPR, all the RPRs under three emission scenarios showed extremely obvious increase trends and similar increase rates during 2011-2040. However, from about 2041 onwards, differences arise and become larger and larger. The RPR tends to be almost constant under the RCP2.6 emission scenario. And it also tends to be stable by the end of this century under the RCP4.5 emission scenario. While it will continue to increase under the RCP8.5 emission scenario. This is consistent with prediction of snow cover in Eurasia by Xia (Xia and Wang 2015). The RPR increase mainly due to the significant increase of rainfall and the significant decrease of snowfall (Guo and Li 2015; Jing et al. 2017). From the above analysis, we can see that if effective greenhouse gas emission reduction policies are implemented, future greenhouse gas emissions could be controlled at a low level. In this way, the RPR in the TMR will change not too much in the future. However, if the greenhouse gas emissions can not be effectively controlled from now, the change of RPR in the short term (2011-2040) maybe not be obvious, but it will become drastic with high probability in the second half of the 21$^{st}$ century as time passes.

It should be pointed out that meteorological stations could provide available data are mainly distributed in region with relatively low altitude. And the observed precipitation data from the high latitude are quite rare. Therefore, it brought uncertainty to this study. In view of this, it is necessary to add more observation stations with high latitude in the future to strengthen the observation of precipitation types in the TMR. In recent years, global precipitation observations based on satellite remote sensing have been gradually improved. It is necessary to deepen the understanding of satellite remote sensing data and choose suitable satellite remote sensing data to study change of precipitation types in the TMR. Also, the assumption that the statistical relationship between variable historical observations and simulated data will still hold in the future also lead to uncertainty in prediction of RPR. In the historical period, the closest relationship between the temperature and change of precipitation types were obtained. However, factors that affect the transformation of precipitation types in the future are not yet clear. Further study will consider more factors as variables to optimize model.

## 6. Conclusions

This study firstly evaluated the ability of the CMIP5 models to simulate temperature and precipitation in the TMR. The CMIP5 models could better reproduce temperature

but not for precipitation. Therefore, the temperature data provided by CMIP5 models and other meteorological factors data were used to simulate and predict RPR by the BNN model.

Under the three emission scenarios (RCP2.6, 4.5, and 8.5), values of RPR in the months experiencing freezing-thawing transitions during the future period (2011-2100) will be higher than that during the historical period (1981-2010) in the TMR. The values of RPR will mostly increase with the rise of RCP emission scenario. In the same emission scenario, The values of RPR increase as the time goes on. This means that the transition from snowfall to rainfall is more obvious. In terms of spatial variation, values of RPR in the south slope were larger than that in the north slope during 1981-2010. The spatial distribution of RPR during 2011-2100 will change not much compared with that during 1981-2010. The increase rate of RPR during the future period will be different from that during the historical period in the TMR. Under the low-emission scenario (RCP2.6), as time goes on, values of RPR at more stations will change slightly. Under the medium-emission scenario (RCP4.5), the increase of RPR will occur in the whole TMR and stabilize in the north slope by the end of this century. Under the high-emission scenario (RCP8.5), values of RPR will increase significantly through 21$^{st}$ century in the whole TMR.

## Acknowledgments

This work was financially supported by the National Natural Science Foundation of China (41761014), the Foundation of A Hundred Youth Talents Training Program of Lanzhou Jiaotong University, and the Excellent platform of Lanzhou Jiaotong University. We are grateful to the Coupled Model Working Group responsible for the World Climate Research Program of CMIP and the climate modeling group (listed in Table 1 of this article) for their efforts to generate model outputs.

## Conflicts of interest

The authors have no conflicts of interest to declare that are relevant to the content of this article.

## Funding Statement

This work was financially supported by the National Natural Science Foundation of China (41761014), the Foundation of A Hundred Youth Talents Training Program of Lanzhou Jiaotong University, and the Excellent platform of Lanzhou Jiaotong University.

## Author's Contribution

All authors contributed to the study conception and design. Material preparation, data collection and analysis were performed by [Rui Ren], [Xuemei Li], [Lanhai Li] and [Yiyu Huang]. The first draft of the manuscript was written by [Rui Ren] and all authors commented on previous versions of the manuscript. All authors read and approved the final manuscript.

## References


Anderson B, Mackintosh A (2012) Controls on mass balance sensitivity of maritime glaciers in the Southern Alps, New Zealand: The role of debris cover. J Geophys Res 117. https://doi.org/117(F1),F01003.10

ASCE (2000) Artificial Neural Networks in Hydrology. I: Preliminary Concepts. J Hydrol Eng 5:115-123. https://doi.org/10.1061/(ASCE)1084-0699(2000)5:2(115)

Chen Y, Li W, Deng H, Fang G, Li Z (2016) Changes in Central Asia's Water Tower: Past, Present and Future. Sci Rep 6:35458. https://doi.org/10.1038/srep35458

Clark MP, Slater AG, Barrett AP, Hay LE, Mccabe GJ, Rajagopalan B, Leavesley GH (2006) Assimilation of snow covered area information into hydrologic and land-surface models. Adv Water Resour 29:1209-1221. https://doi.org/10.1016/j.advwatres.2005.10.001

Cohen J, Rind D (1991) The Effect of Snow Cover on the Climate. J Clim 4:689-706. https://doi.org/10.1175/1520-0442(1991)0042.0.CO;2

Dai, Aiguo (2008) Temperature and pressure dependence of the rain-snow phase transition over land and ocean. Geophys Res Lett 35:62-77. https://doi.org/10.1029/2008GL033295

Dandan HE, Changchun XU, Jingchao L, Jinping HE (2018) Future Climate Scenarios Projection in the Kaidu River Basin Based on ASD Statistical Downscaling Model. Pearl River 39:25-32. (in Chinese with English abstract)

Ding BD, Baohong, Yang KY, Kun, Qin JQ, Jun, Wang LW, Lei, Chen YC, Yingying, He XH, Xiaobo (2014) The dependence of precipitation types on surface elevation and meteorological conditions and its parameterization. J Hydrol Eng 513:154-163. https://doi.org/10.1016/j.jhydrol.2014.03.038

Feng S, Hu Q (2004) Changes in agro-meteorological indicators in the contiguous United States: 1951-2000. J Hydrol Eng 78:p. 247-264. https://doi.org/10.1007/s00704-004-0061-8

Ghosh KG (2018) Analysis of Rainfall Trends and its Spatial Patterns During the Last Century over the Gangetic West Bengal, Eastern India. JGSA 2. https://doi.org/10.1007/s41651-018-0022-x

Guo L, Li L (2015) Variation of the proportion of precipitation occurring as snow in the Tian Shan Mountains, China. Int J Climatol 35:1379-1393. https://doi.org/10.1002/joc.4063

Gupta HV, Sorooshian S, Yapo PO (1999) Status of Automatic Calibration for Hydrologic Models: Comparison With Multilevel Expert Calibration. J Hydrol Eng 4:135-143. https://doi.org/10.1061/(ASCE)1084-0699(1999)4:2(135)

Han C, Chen R, Liu J, Yang Y, Qing W (2010) A Discuss of the Separating Solid and Liquid Precipitations. Journal of Glaciology and Geocryology 32:249-256. (in Chinese with English abstract)

Hay LE, Wilby RL, Leavesley GH (2010) A COMPARISON OF DELTA CHANGE AND DOWNSCALED GCM SCENARIOS FOR THREE MOUNTAINOUS BASINS IN THE UNITED STATES1. J Am Water Resour Assoc 36:387-397. https://doi.org/387-397.10.1111/j.1752-1688.2000.tb04276.x

Hu R (2004) Physical Geography of the Tianshan Mountains in China. China Environmental Science Press, Beijing. (in Chinese with English abstract)

Huang Y, Yan Q, Zhang C (2018) Spatial–Temporal Distribution Characteristics of PM2.5 in China in 2016. JGSA 2. https://doi.org/10.1007/s41651-018-0019-5

Hussain M, Yusof KW, Mustafa MRU, Mahmood R, Jia S (2017) Evaluation of CMIP5 models for projection of future precipitation change in Bornean tropical rainforests. Theor Appl Climatol 134:423-440. https://doi.org/10.1007/s00704-017-2284-5

IPCC (2013) Climate Change 2013: the Physical Science Basis. Contribution of Working Group I to the Fifth Assessment Report of the Intergovernmental Panel on Climate Change. Cambridge University Press, Cambridge, United Kingdom, New York, NY, USA

IPCC, Matthews R, Babiker M, Coninck HD, Weyer NM (2018) Annex I: Glossary. In: Global warming of 1.5°C. An IPCC Special Report.

Ji F, Wu Z, Huang J, Chassignet E (2014) Evolution of land surface air temperature trend. Nat clim Change 4:462-466. https://doi.org/10.1038/nclimate2223

Jing Y, Gonghuan F, Yaning C, De-Maeyer P (2017) Climate change in the Tianshan and northern Kunlun Mountains based on GCM simulation ensemble with Bayesian model averaging. J Arid Land 9:622-634. https://doi.org/10.1007/s40333-017-0100-9

Knowles N, Dettinger MD, Cayan DR (2006) Trends in Snowfall versus Rainfall in the Western United States. Clim Change 19.https://doi.org/10.1175/JCLI3850.1

Li et al. (2015) Temporal and spatial variation of 10-day mean air temperature in Northwestern China Theoretical & Applied Climatology

Li Q, Yang T, Zhang F, Qi Z, Li L (2019) Snow depth reconstruction over last century: Trend and distribution in the Tianshan Mountains, China. Glob Planet Change 173:73-82. https://doi.org/10.1016/j.gloplacha.2018.12.008

Li x, Gao P, li Q, Tang H (2016) Muti-paths Impact from Climate Change on Snow Cover in Tianshan Mountainous Area of China. Advances in Climate Change Research 12:303-312 (in Chinese with English abstract)

Loth B, Graf HF, Oberhuber JM (1993) Snow cover model for global climate simulations. J Geophys Res-Atmos 98:10451-10464. https://doi.org/10.1029/93JD00324

Lu H, Wei WS, Liu MZ, Han X, Li M, Hong W (2016) Variations in seasonal snow surface energy exchange during a snowmelt period: an example from the Tianshan Mountains, China. Meteorol Appl 23:14-25. https://doi.org/10.1002/met.1511

Lu Z, Zhao T, Zhou W (2020) Evaluation of the Antarctic Circumpolar Wave Simulated by CMIP5 and CMIP6 Models. Atmosphere 11:931. https://doi.org/10.3390/atmos11090931

Moriasi DN, Arnold JG, Liew MWV, Bingner RL, Harmel RD, Veith TL (2007) Model Evaluation Guidelines for Systematic Quantification of Accuracy in Watershed Simulations. Trans ASABE 50:885-900. https://doi.org/10.13031/2013.23153

Nash JE, Sutcliffe JV (1970) River flow forecasting through conceptual models part I — A discussion of principles - ScienceDirect. J Hydrol 10:282-290. doi: https://doi.org/10.1016/0022-1694(70)90255-6

Noor M, Ismail TB, Shahid S, Ahmed K, Chung ES, Nawaz N (2019) Selection of CMIP5 multi-model ensemble for the projection of spatial and temporal variability of rainfall in peninsular Malaysia. Theor Appl Climatol 138:999-1012. https://doi.org/10.1007/s00704-019-02874-0

Ogunbode CA, Doran R, Bhm G (2019) Exposure to the IPCC special report on 1.5 °C global warming is linked to perceived threat and increased concern about climate change. Clim Change 158. https://doi.org/10.1007/s10584-019-02609-0

Qi X, Li W, Li H, Liu H (2017) Future climate change prediction of arid inland river basin based on CMIP5 model. Arid Land Geography 40:987-996. (in Chinese with English abstract)

Rui R, Xuemei LI, Lanhai LI, Qirui Q, Yiyu H (2020) Discrimination of driving factors of precipitation forms in Tianshan Mountains area of China. Journal of Arid Land Resources and Environment 34:112-117.(in Chinese with English abstract)

Rumelhart DE, Hinton GE, Williams RJ (1986) Learning representations by back-propagating errors. Nature 323:533-536. https://doi.org/10.1016/B978-1-4832-1446-7.50035-2

Wang L, Liu HL, Bao AM, Pan XL (2014) Estimating the sensitivity of runoff to climate change in an alpine-valley watershed of Xinjiang, China. Hydrolog Sci J 61. https://doi.org/10.1080/02626667.2014.964718

Wei H, Cunde X, Tingfeng D, Minghu D (2018) Changes in the Proportion of Precipitation Occurring as Rain in Northern Canada during Spring–Summer from 1979–2015. Adv Atmos Sci v.35:31-38. https://doi.org/10.1007/s00376-018-7226-3

Xia K, Wang B (2015) Evaluation and projection of snow cover fraction over Eurasia. Climatic and Environmental Research 20:41-52. (in Chinese with English abstract)

Xu L, Zhu M, He B, Wang X, Zhang Q, Jiang J, Razafindrabe BHN (2014) Analysis of Water Balance in Poyang Lake Basin and Subsequent Response to Climate Change. J Coast Res 68:136-143. https://doi.org/10.2112/SI68-018

Ye, Hengchun (2008) Changes in Frequency of Precipitation Types Associated with Surface Air Temperature over Northern Eurasia during 1936–90. J Clim 21:5807-5819. https://doi.org/10.1175/2008JCLI2181.1

# Figures

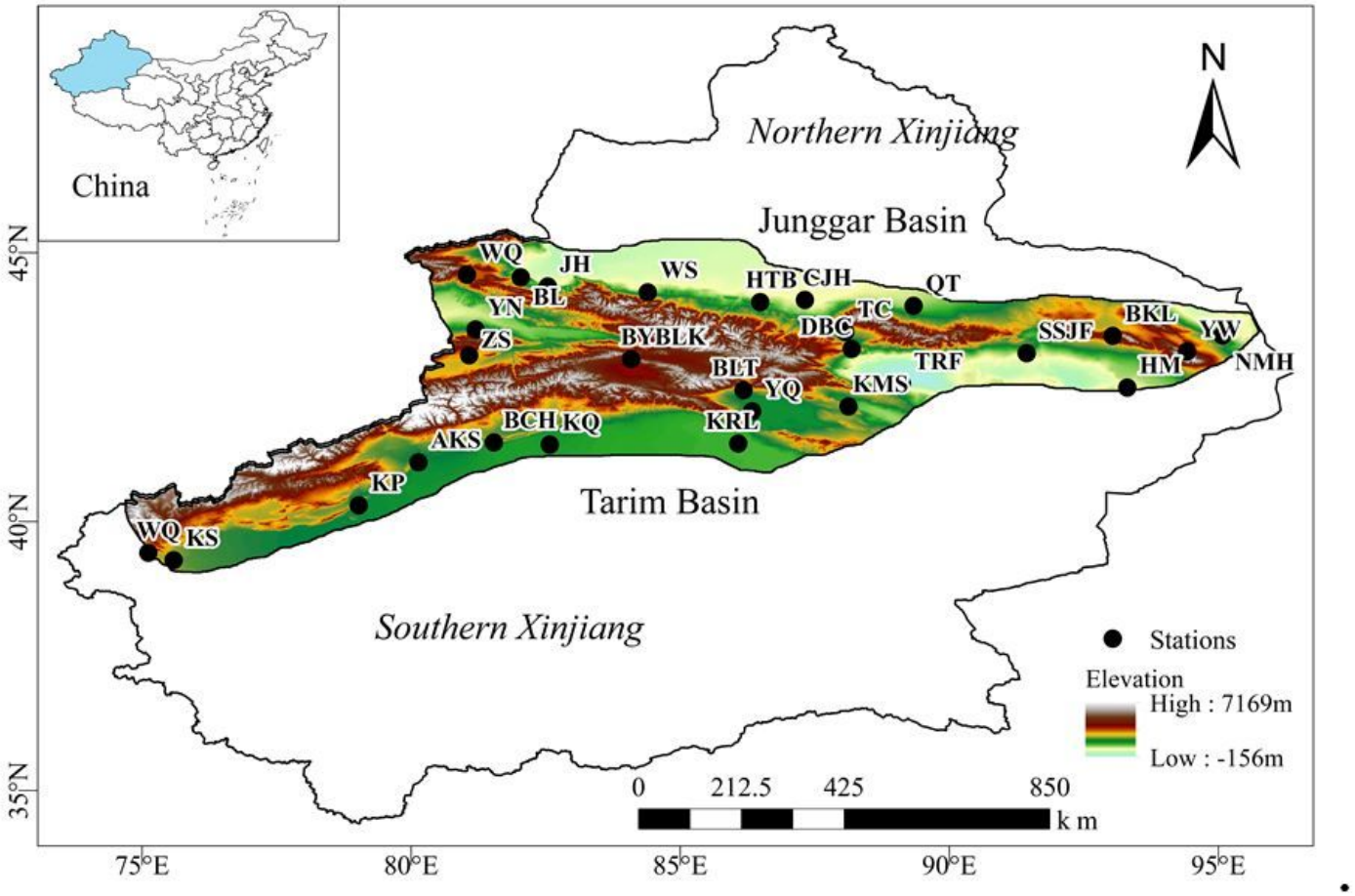


**Figure 1**

Map of the TMR and the distribution of selected meteorological stations Note: The designations employed and the presentation of the material on this map do not imply the expression of any opinion whatsoever on the part of Research Square concerning the legal status of any country, territory, city or area or of its authorities, or concerning the delimitation of its frontiers or boundaries. This map has been provided by the authors.

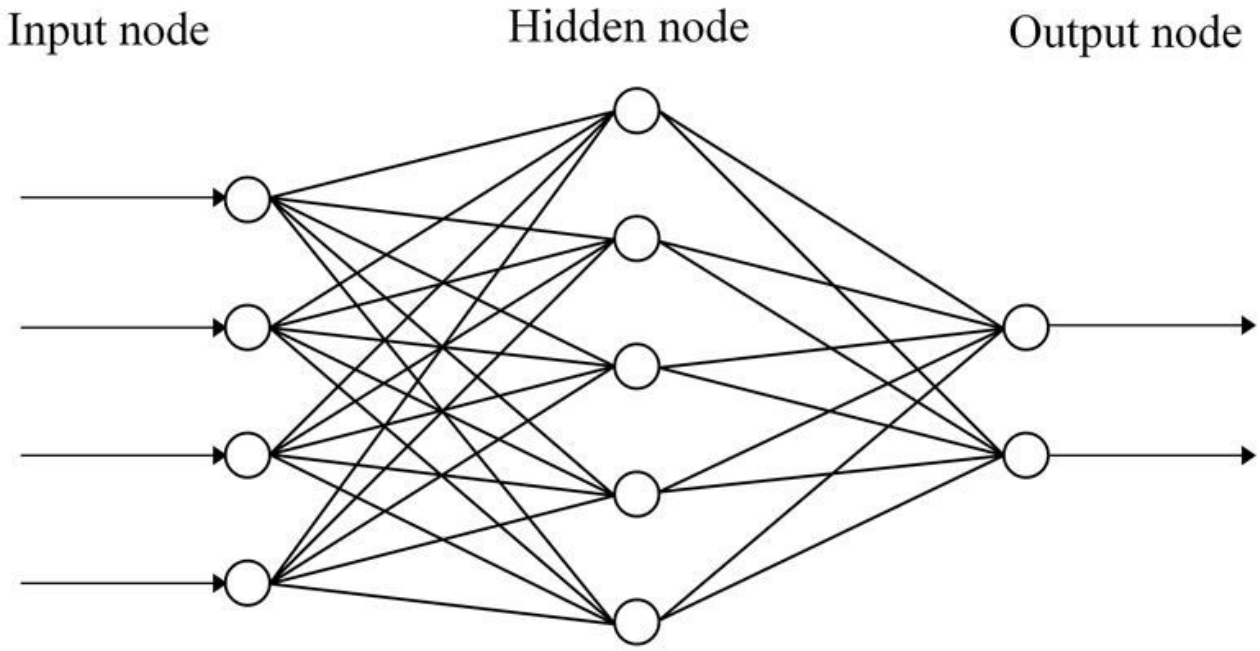


Figure 2

Learning representations by back-propagating errors

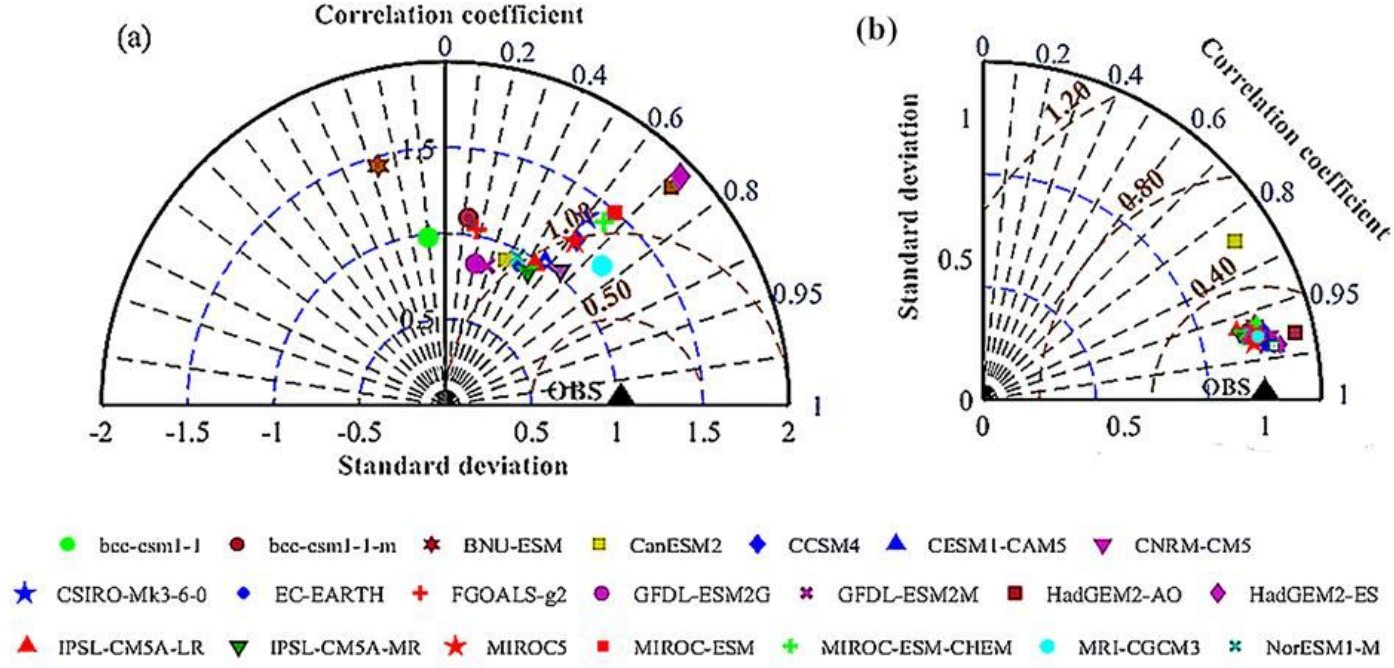


Figure 3

Taylor Diagram of the 21 CMIP5 models simulated fields and the observed fields: (a) annual precipitation and (b) annual mean temperature during period (1961- 2018) in TMR

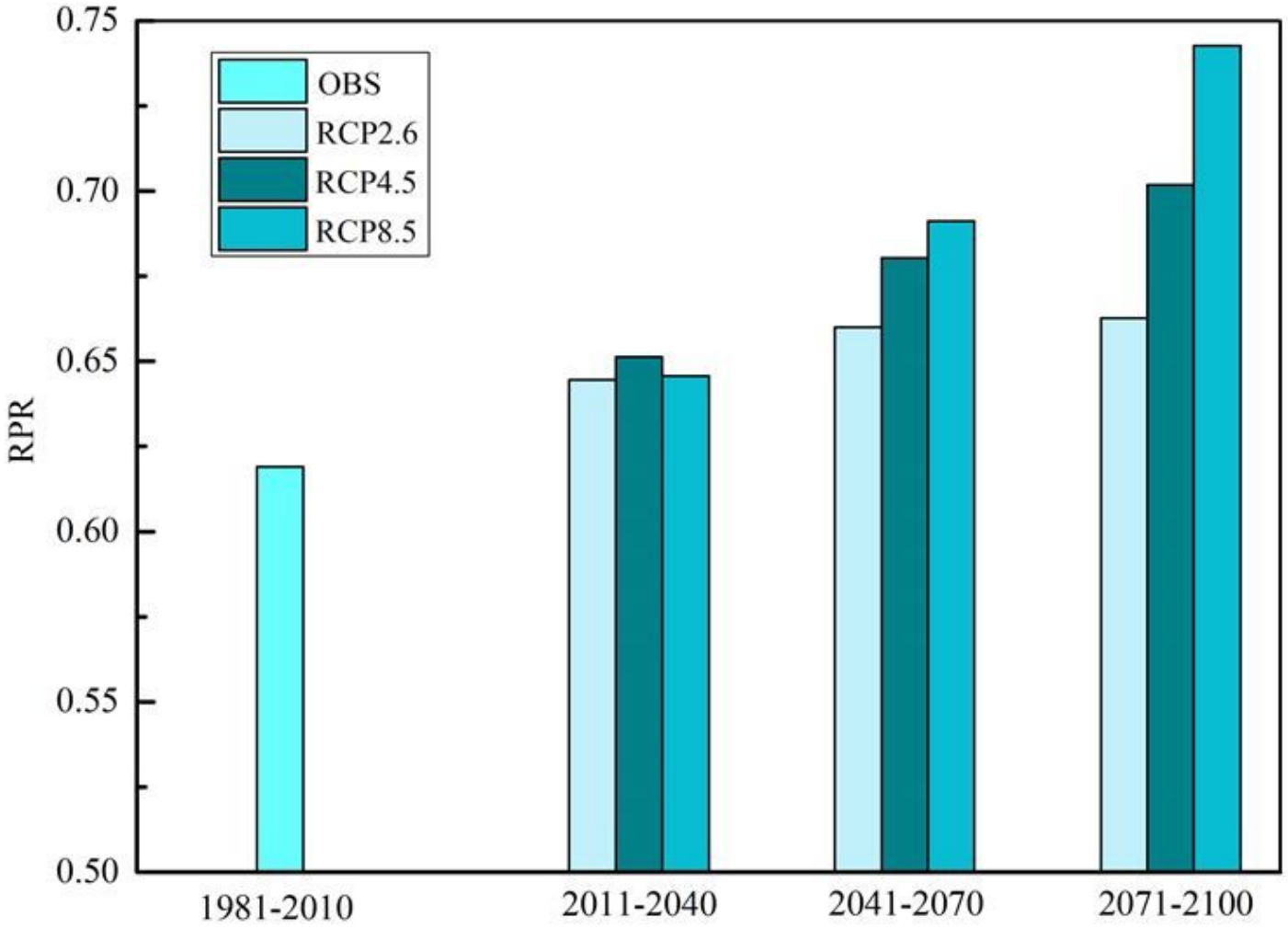


**Figure 4**

RPR in the months experiencing freezing-thawing transitions under different scenarios (RCP2.6, 4.5, and 8.5) in the TMR

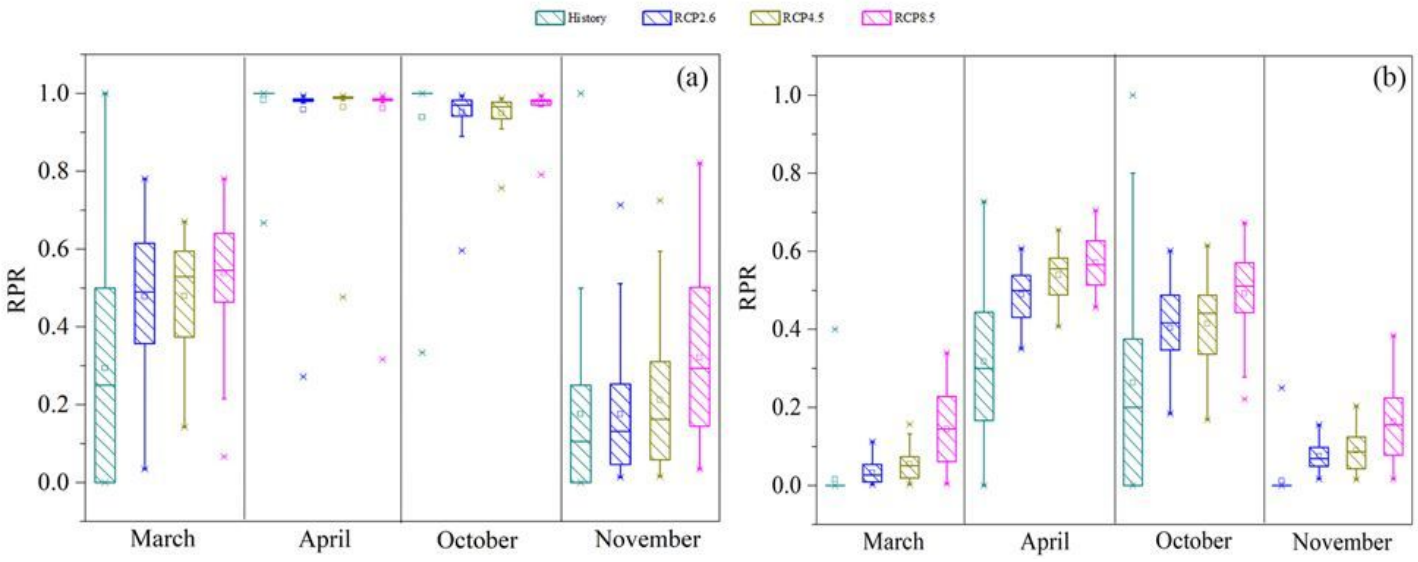


**Figure 5**

Box plots of RPR under three emission scenarios at (a) Bole and (b) Tianchi station during historical periods (1981-2010) and the future periods (2071-2100)

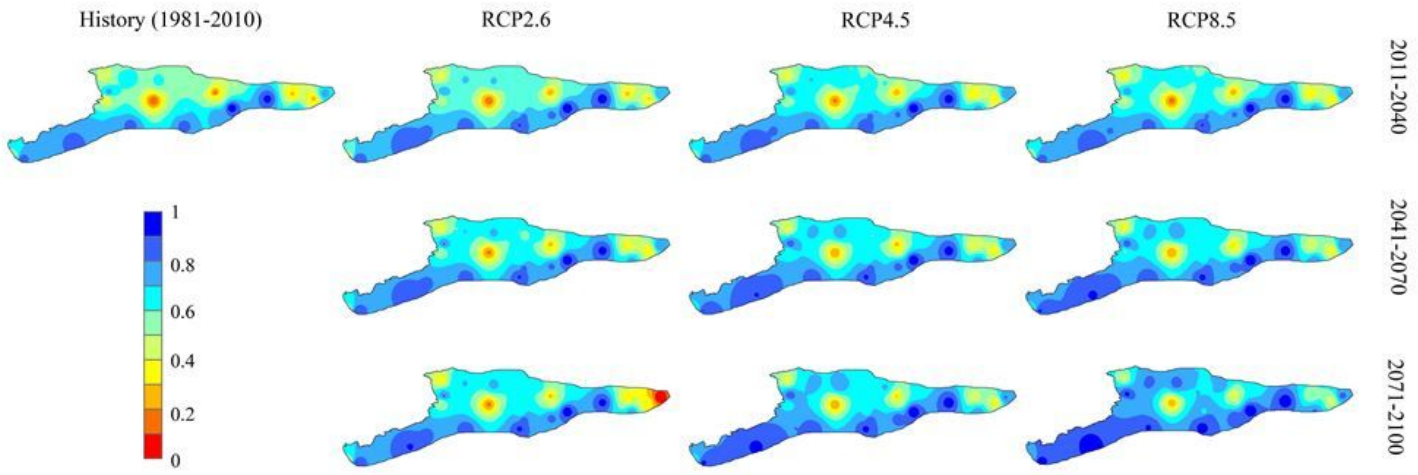


**Figure 6**

Spatial distribution of RPR in the months experiencing freezing-thawing transitions under RCP2.6, 4.5, and 8.5 emission scenario in the TMR Note: The designations employed and the presentation of the material on this map do not imply the expression of any opinion whatsoever on the part of Research Square concerning the legal status of any country, territory, city or area or of its authorities, or concerning the delimitation of its frontiers or boundaries. This map has been provided by the authors.

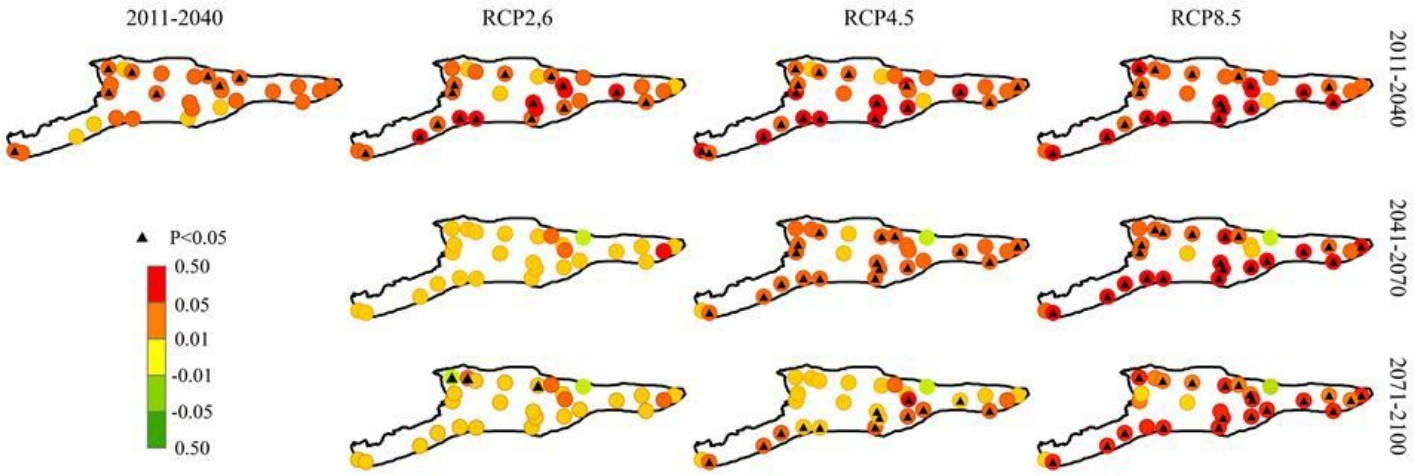


## Figure 7

Spatial distribution of changing trend of RPR in the months experiencing freezing-thawing transitions in TMR under the three emission scenarios (RCP2.6, 4.5, and 8.5) Note: The results have passed the 95% reliability t-test (black triangle) Note: The designations employed and the presentation of the material on this map do not imply the expression of any opinion whatsoever on the part of Research Square concerning the legal status of any country, territory, city or area or of its authorities, or concerning the delimitation of its frontiers or boundaries. This map has been provided by the authors.